

This discussion paper is/has been under review for the journal Atmospheric Chemistry and Physics (ACP). Please refer to the corresponding final paper in ACP if available.

A Lagrangian view of convective sources for transport of air across the Tropical Tropopause Layer: distribution, times and the radiative influence of clouds

A. Tzella and B. Legras

Laboratoire de Météorologie Dynamique, CNRS, UMR8539, Ecole Normale Supérieure, 24 rue Lhomond, Paris, 75005, France

Received: 14 June 2011 – Accepted: 18 June 2011 – Published: 24 June 2011

Correspondence to: A. Tzella (tzella@imd.ens.fr)

Published by Copernicus Publications on behalf of the European Geosciences Union.

A Lagrangian view of transport across the TTL

A. Tzella and B. Legras

Title Page

Abstract

Introduction

Conclusions

References

Tables

Figures

◀

▶

◀

▶

Back

Close

Full Screen / Esc

Printer-friendly Version

Interactive Discussion



Abstract

The Tropical Tropopause Layer (TTL) is a key region controlling transport between the troposphere and the stratosphere. The efficiency of transport across the TTL depends on the continuous interaction between the large-scale advection and the small-scale intermittent convection that reaches the Level of Zero radiative Heating (LZH). The wide range of scales involved presents a significant challenge to determine the sources of convection and quantify transport across the TTL. Here, we use a simple Lagrangian model, termed *TTL detrainment model*, that combines a large ensemble of 200-day back trajectory calculations with high-resolution fields of brightness temperatures (provided by the CLAUS dataset) in order to determine the ensemble of trajectories that are detrained from convective sources. The trajectories are calculated using the ECMWF ERA-Interim winds and radiative heating rates, derived both under all-sky and clear-sky conditions, so that the radiative influence of clouds is established.

We show that most trajectories are detrained near the mean LZH with the horizontal distributions of convective sources being highly-localized, even within the space defined by deep convection. As well as modifying the degree of source localization, the radiative heating from clouds facilitates the rapid upwelling of air across the TTL. However, large-scale motion near the fluctuating LZH can lead a significant proportion of trajectories to alternating clear-sky and cloudy regions, thus generating a large dispersion in the vertical transport times. The distributions of vertical transport times are wide and skewed and are largely insensitive to a bias of about ± 1 km (∓ 5 K) in the altitude of cloud top heights (the main sensitivity appearing in the times to escape the immediate neighbourhood of the LZH) while seasonal and regional transport characteristics are only apparent at small time-scales. The strong horizontal mixing that characterizes the TTL ensures that most air of convective origin is well-mixed within the tropical and eventually within the extra-tropical lower-stratosphere.

ACPD

11, 18161–18209, 2011

A Lagrangian view of transport across the TTL

A. Tzella and B. Legras

Title Page

Abstract

Introduction

Conclusions

References

Tables

Figures

◀

▶

◀

▶

Back

Close

Full Screen / Esc

Printer-friendly Version

Interactive Discussion



1 Introduction

It is now widely accepted that most of the transport of tropospheric air into the stratospheric “overworld” at potential temperatures above about 380 K takes place in the tropics (see reviews by Holton et al., 1995; Stohl et al., 2003), across what is now known as the Tropical Tropopause Layer (TTL) (see Highwood and Hoskins, 1998; Folkens et al., 1999; Fueglistaler et al., 2009a). This layer, whose vertical extent is over several kilometres, spans the gradual transition from a region dominated by the convectively overturning motion of the Hadley-Walker circulation to a region of slow ascent, controlled by the tropical branch of the Brewer-Dobson circulation. The efficiency at which air is transported across the TTL depends on both the large-scale advection and the local sources of deep convection. A detailed quantification of their combined effect is challenging because of the large range of scales involved. Such a quantification is particularly important for halogenated Very Short-Lived Substances (VSLS) whose impact on ozone depletion relies on their efficient transport into the stratosphere (see e.g., WMO, 2007).

Air from the boundary layer is rapidly (within hours) transported into the TTL by deep convection. The latter frequently penetrates the region near the TTL base, commonly taken to lie above the level of maximum convective outflow (between 345–355 K, 12–14 km; see e.g., Gettelman and de Forster, 2002; Fueglistaler et al., 2009a). However, most air detrained in this region descends back to the boundary layer. With increasing altitude, convection becomes increasingly rare (see e.g., Liu and Zipser, 2005; Fu et al., 2007). As a result, the magnitude of the radiative cooling outside the clouds decreases leading to a smaller descending mass-flux. This decrease continues up until a certain level, situated at about 360 K (15 km), that marks the transition from clear-sky radiative cooling to radiative heating (Gettelman et al., 2004). Once above this level, known as the Clear sky Level of Zero radiative Heating (C-LZH), the majority of air originating from deep convection is transported into the stratosphere.

A Lagrangian view of transport across the TTL

A. Tzella and B. Legras

Title Page

Abstract

Introduction

Conclusions

References

Tables

Figures



Back

Close

Full Screen / Esc

Printer-friendly Version

Interactive Discussion



A Lagrangian view of transport across the TTL

A. Tzella and B. Legras

Title Page

Abstract

Introduction

Conclusions

References

Tables

Figures

◀

▶

◀

▶

Back

Close

Full Screen / Esc

Printer-friendly Version

Interactive Discussion



The mean 5–15 K (1–3 km) gap between the level of maximum convective outflow and the mean C-LZH implies that the number of convective sources that can penetrate the C-LZH is potentially too small to explain the large-scale upward mass-flux in the Brewer-Dobson circulation. This discrepancy is accounted for by considering the radiative influence of thin, high cirrus clouds. The latter are omnipresent in the TTL (e.g., Wang et al., 1996; Martins et al., 2011), generated either from the outflow of deep convective anvils or in situ (e.g., Massie et al., 2002), with lifetimes of a few days, reaching horizontal scales of the order of 1000 km (e.g., Winker and Trepte, 1998). Using a large number of detailed radiative transfer calculations to quantify upwelling and subsidence in cloudy and cloud-free air, Corti et al. (2005) showed that the All-sky Level of Zero radiative Heating (A-LZH) is on average about ~ 355 K (14 km), i.e., ~ 5 K (1 km) lower than the C-LZH. The gap between the A-LZH and the mean level of maximum convective outflow is thus reduced, facilitating a larger proportion of air to be transported into the stratosphere. The net radiative heating associated with cirrus clouds (which within cirrus clouds is ~ 1 K day⁻¹) allows for the rapid transport of air upwards, up to the C-LZH, above which their radiative influence becomes increasingly small. According to Corti et al. (2006), it can take as little as two weeks (a time sufficiently short for most VSLS) for air of convective origin to reach the 370 K surface, if this remains inside cirrus clouds for most of the time.

The above descriptions and estimates are based on mean vertical profiles and thus do not take into account the detailed pathways of cloud air (i.e., air originating from deep convection). These pathways are largely controlled by large-scale horizontal advection that, in this region of the atmosphere, can transport cloud air along great longitudinal distances (see Holton and Gettelman, 2001; Fueglistaler et al., 2004; Bonazzola and Haynes, 2004). Horizontal transport could play a significant role in the vertical transport of cloud air into the stratosphere. Because clouds are spatially localized and intermittent, both the heating rates and the A-LZH are highly fluctuating in space and time. In contrast, in clear-sky, the distributions of heating rates are smoother. Horizontal motion can thus transport cloud air that is detrained within a certain region into other

regions, with very different vertical heating rate profiles. As a result, cloud air detrained above the A-LZH may subside back into the troposphere or remain for a long time near the A-LZH so that its motion is fluctuating in the vertical direction. The combined effect of the radiative heating associated with clouds and the large-scale horizontal flow for transport of air of convective origin into the stratosphere is a priori unknown.

To examine this effect, in this paper we use a simple Lagrangian model, termed *TTL detrainment model*, that combines a large number of back trajectory calculations, initially located within the upper TTL, with high-resolution global fields of brightness temperatures. Our particular focus is to determine the ensemble of trajectories that are detrained from deep convection. This ensemble is then used to deduce the distribution of convective sources and times for transport of cloud air across the TTL. The trajectories are calculated using the European Centre of Medium range Weather Forecast (ECMWF) ERA-Interim (EI) re-analysis winds and radiative heating rates, derived both under all-sky and clear-sky conditions so that the radiative influence of clouds is established. The brightness temperature data are obtained from the CCloud Archive User Service (CLAUS). In order to evaluate the sensitivity of the results to biases in the brightness temperatures, BT, we consider a variable offset of $\Delta T = \pm 5$ K.

In the next section we present the model, data and trajectory calculations used in this study. In Sect. 3 we present our results. We last conclude in Sect. 4.

2 Data and method: the TTL detrainment model

2.1 Trajectory calculations

We employ large-scale wind and temperature fields to calculate an ensemble of back trajectories whose initial positions are uniformly distributed on two iso-pressure surfaces that lie in the upper TTL: 100 hPa and 70 hPa. The trajectories are initialised between 50° N and 50° S, at all longitudes, on a high-resolution $1^\circ \times 1^\circ$ longitude/latitude grid (36 360 trajectories) and followed backward-in-time for 200 days. This range of

A Lagrangian view of transport across the TTL

A. Tzella and B. Legras

Title Page

Abstract

Introduction

Conclusions

References

Tables

Figures

◀

▶

◀

▶

Back

Close

Full Screen / Esc

Printer-friendly Version

Interactive Discussion



latitudes encompasses the latitude range of the TTL in all seasons. The trajectories are initialised at 12:00 UTC every 4 days covering the period between the 1 January 2005 to the 30 June 2006, resulting a total of 5 017 680 (138 × 36 360) trajectories. We use these back trajectories to investigate the characteristics of convective sources for transport of cloud air across the TTL. A main motivation lies in understanding how these sources influence the distributions of VSLs in the upper TTL. Their lifetimes are by definition less than 6 months (see e.g., WMO, 2007). Therefore, 200-day simulations are both sufficient and necessary for our purposes.

The back trajectories are computed in an isentropic coordinate system with TRACZILLA, a modified version of FLEXPART (Stohl et al., 2005; Pisso and Legras, 2008), using analysis (at 00:00, 06:00, 12:00 and 18:00 UTC) and 3-h forecasts (at 03:00, 09:00, 15:00, and 21:00 UTC) from the European Centre of Medium range Weather Forecast (ECMWF) ERA-Interim (EI) re-analysis dataset (T255 spectral resolution, 60-level hybrid vertical coordinates and 12-h 4D-Var assimilation; see Dee et al., 2011). Diabatic trajectories have been found to be less dispersive than trajectories obtained by kinematic models in which transport is derived from three-dimensional wind fields (e.g., Schoeberl et al., 2003; Stohl et al., 2004; Wohltmann and Rex, 2008), though this difference is less prominent in the EI dataset (Liu et al., 2010).

The horizontal (isentropic) part of the motion is obtained from the meteorological wind fields. First extracted on a $1^\circ \times 1^\circ$ longitude/latitude grid, the wind fields are linearly interpolated in the latitude, longitude and log-pressure along the trajectories. Trajectories are then integrated in time with a 15 min time-step. The vertical (cross-isentropic) part of the motion is derived from *radiative heating rates*, Q_{rad} , provided as 3-h averages from forecasts of temperature tendencies. The vertical displacement is then given by

$$\frac{d\theta}{dt} = \frac{\theta}{c_p T} Q_{\text{rad}}, \quad (1)$$

where θ denotes potential temperature, T temperature and c_p the specific heat capacity per unit mass at constant pressure. In general, this part of the motion is derived

A Lagrangian view of transport across the TTL

A. Tzella and B. Legras

Title Page

Abstract

Introduction

Conclusions

References

Tables

Figures

◀

▶

◀

▶

Back

Close

Full Screen / Esc

Printer-friendly Version

Interactive Discussion



from diabatic heating rates whose values can also depend on additional processes to radiative heating. However, as long as a trajectory remains in cloud-free air, the component of heating that is associated with the release of latent heat can be discarded while the contribution of heat transfer by turbulent motion and diffusion was previously found to be small (Fueglistaler et al., 2009b).

The radiative heating rates can be calculated in both clear-sky and all-sky conditions in which case the radiative effect of different kind of clouds is included. Calculating the contribution of clouds on the radiative heating rates can become quite involved, particularly in regions where both optically thick anvil clouds and thin cirrus clouds co-exist. The uncertainties in the radiative heating rates are thus larger in the lower TTL (see Fig. 7 in Fueglistaler et al., 2009b). Note that the contribution of clouds to the radiative heating rates is, within the ECMWF model, obtained using statistical assumptions about the cloud distribution within the mesh. This calculation can thus not distinguish between the heating occurring inside the clouds from that occurring outside the clouds. We assume that as long as the trajectories are situated above deep convective clouds, the cloud component of the radiative heating is related to the external effect of clouds.

As noted in the introduction, cirrus clouds can enhance the net tropical radiative heating rates. This enhancement is reflected in the annual mean vertical tropical profiles of the radiative heating rates, shown in Fig. 1a, obtained for clear-sky and all-sky conditions from the EI dataset for 2005. The differences between the two profiles result in different estimates for the transit time between an initial level in potential temperature, θ_0 , and the 380 K level (see Fig. 1b). These differences are especially important below 365 K where the estimated transit time is strongly dependent on the value of θ_0 , diverging as θ_0 approaches the mean LZH (in either clear- or all-sky conditions) that acts as a barrier for transport between the lower and upper troposphere.

The above estimates do not take into account the horizontal part of the motion. They nevertheless point to the key role that cloud radiation has on transport across the TTL. In order to obtain a comprehensive quantification of the radiative influence of

A Lagrangian view of transport across the TTL

A. Tzella and B. Legras

Title Page

Abstract

Introduction

Conclusions

References

Tables

Figures



Back

Close

Full Screen / Esc

Printer-friendly Version

Interactive Discussion



cirrus clouds on transport across the TTL, we here consider both all-sky and clear-sky radiative heating rates for the vertical part of the motion. Such a quantification has to some extent been examined in Ploeger et al. (2010) where it is found that vertical transport is indeed faster when the radiative influence of clouds is taken into account.

5 This study, however, focuses on back trajectories arriving on fixed levels of θ_0 that are not related to the potential temperature at which air of convective origin detrains.

Note that it is possible that some air parcels remain for a long time in the immediate neighbourhood of the launch surface. As a result, their contribution could be overestimated with respect to the remaining parcels. These spurious contributions can be important if the proportion of these parcels is large. The latter depends on the frequency at which the trajectories are launched. The higher is this frequency, the larger is the proportion of air parcels remaining in the immediate neighbourhood of the launch surface within the next launch. This dependence on the launch frequency is the main reason why trajectory calculations cannot be used to determine fluxes across a surface. In order to estimate the importance of these spurious contributions, we calculate the percentage of air parcels that move upwards and downwards for a number of days (1, 2, ..., 8) after their launch at 100 hPa. We find that after two days, the proportion of air parcels that move upwards has stabilised (the proportions vary by less than 2%). The same happens for the proportion of air parcels that move downwards. We can therefore conclude that by the time the new set of trajectories is launched (4 days after), the proportion of air parcels that have remained in the immediate neighbourhood of the initial launch level is negligible. We therefore expect that the above mentioned spurious contributions are insignificant for the launch frequency that we here employ.

2.2 Detrainment

25 Our main aim is to determine and characterise the sub-ensemble of trajectories that have encountered convective sources, thereafter called the CS-TTL ensemble. To that end, we employ high-resolution fields of cloud top heights, estimated using satellite brightness temperature (BT) measurements based on the infra-red window (mean

A Lagrangian view of transport across the TTL

A. Tzella and B. Legras

Title Page

Abstract

Introduction

Conclusions

References

Tables

Figures



Back

Close

Full Screen / Esc

Printer-friendly Version

Interactive Discussion



11 μm channel), obtained from the CCloud Archive User Service (CLAUS) at $1/3^\circ \times 1/3^\circ$ spatial resolution and 3-h temporal resolution (Hodges et al., 2000) that are mapped along the trajectories using piecewise constant interpolation. The use of brightness temperatures to measure cloud top heights is based on the standard assumption that the temperature at the top of the cloud is equal to that of the environment at this location.

Note that CLAUS maps all types of clouds. However, here, we are only interested by the anvils produced by deep convection. This distinction cannot be made in the absence of available cloud classification at a global scale or information from other channels. The presence of high-altitude, semi-transparent cirrus situated above the anvil may therefore introduce a possible bias in the cloud top heights. Other biases are related to the non-equilibrium evolution of the cloud that lead to temperature differences and cloud heterogeneity within the pixel (Sherwood et al., 2004). In order to take into account these sort of biases, we consider a variable offset, ΔT , to the brightness temperatures that ranges within the $\pm 5\text{ K}$ interval (see Sect. 2.3 for more details on the CS-TTL ensembles that we obtain).

A trajectory is identified as a member of the CS-TTL ensemble if the time history of its temperature over the duration of the back-trajectory has at some point been larger than the temperature on the top of the cloud. In this case, the last encounter with a cloud is given by the first time (in backward time) at which the parcel's temperature becomes larger than the cloud top temperature.

For the above rule to be well-posed, the cloud top height needs to be unambiguously defined in terms of temperature. This is indeed the case within the tropics where the temperature decreases monotonically with height until a distinct minimum is reached at approximately 380 K. We therefore impose two further rules. The first rule is that the parcel's potential temperature at the encounter point is less than 380 K i.e., the position of the air parcel at this point lies below the tropical tropopause. The second rule is that the parcel's latitudinal position at the encounter point is constrained within (30° S , 30° N) except for the boreal summer season during which it is constrained within

A Lagrangian view of transport across the TTL

A. Tzella and B. Legras

Title Page

Abstract

Introduction

Conclusions

References

Tables

Figures



Back

Close

Full Screen / Esc

Printer-friendly Version

Interactive Discussion



(30° S, 35° N). In practice, the precise value of these boundaries is not important (less than 5 % of the trajectories are detected to encounter a cloud at higher latitudes). At the same time, the northward extension of the northern boundary during boreal summer reflects the presence of the East Asian Monsoon that drives continental convection towards higher latitudes.

The primary consequence of our algorithm is to eliminate the spurious encounters of trajectories with clouds in the stratosphere. For it is now recognised that convective events that penetrate the tropopause are rare, representing less than 0.5 % of the total number of convective events (Liu and Zipser, 2005; Fu et al., 2007) and are therefore unlikely to affect the total transport of mass across the tropopause. A quantity that could be more sensitive to overshooting events is the distribution of water vapour. However, it is now established that in the lower stratosphere, its distribution can be successfully reconstructed using large-scale wind and temperature fields, both globally (see e.g., Fueglistaler et al., 2005; James et al., 2008; Liu et al., 2010) and locally (Schiller et al., 2009). This suggests that most of its variability is controlled by slow dehydration induced by the large-scale motion.

The here described model, that we refer to as the *TTL detrainment model*, was previously introduced, within a different context, by Nawrath (2002) and James et al. (2008) to reconstruct distributions of water vapour in both the troposphere and the stratosphere. In this paper, we use this model as a way to identify the global distribution of convective sources and times for transport of cloud air across the TTL. This distribution is closely related to the distribution of sources in the boundary layer. At the same time, the distribution of times for transport of air into the upper TTL is expected to be similar for air originating from the boundary layer and air originating from the sources of convection. This is because the parcels' motion between the boundary layer and the point of detrainment is characterised by a rapid, vertical upward transfer that lasts several minutes (or at most several hours in the case of a thick anvil). Making the general assumption that the parcels that reach heights near the cloud top are those parcels that are least diluted by entrainment of environmental air, we deduce that, at the point

A Lagrangian view of transport across the TTL

A. Tzella and B. Legras

Title Page

Abstract

Introduction

Conclusions

References

Tables

Figures



Back

Close

Full Screen / Esc

Printer-friendly Version

Interactive Discussion



of detrainment, the CS-TTL parcels' composition in non-soluble tracers is similar to the composition of the boundary layer at the same horizontal location.

We note that a modified version of the TTL detrainment model was recently employed by Wright et al. (2011) to examine the relative contribution to stratospheric water vapour of different regions within South-East Asia during boreal summer. The main modification appears in the vertical motion of the trajectories: instead of radiative heating rates, Wright et al. (2011) employed total diabatic heating rates. The effect of this modification is now discussed.

The rapid upward convective motion between the boundary layer and detrainment occurs over sub-grid horizontal scales of a few kilometres. This motion is parameterized within the ECMWF model and averaged within the mesh. The resolved vertical velocity or, equivalently, the total diabatic heating rate (including the release of latent heat), is, within the regions of convection, positive between the boundary layer and the tropopause. Thus, the descending air parcel motions associated with clear-sky regions between deep convective clouds are not represented. This lack of representation may lead to erroneous transport in the convective regions of the tropical troposphere. This is particularly true for air parcels wandering around the fluctuating A-LZH. Conversely, this lack of representation is likely to be less important for reconstructions of stratospheric water vapour. This is because the latter depend on dehydration events that are now known to occur at altitudes that are, on average, higher (by about 15 K) than the points of detrainment (see James et al., 2008). At these altitudes, latent heat releases are negligible and thus the total diabatic and radiative heating rates are approximately equal (see also Fueglistaler et al., 2009b).

2.3 CS-TTL trajectory ensembles and their characteristics

For each initial level, we run two sets of simulations. The first one is run using all-sky (ALLSKY) radiative heating rates and the second one using clear-sky (CLRSKY) radiative heating rates. For the all-sky simulations, we consider a variable offset to the brightness temperature of $\Delta T = \pm 5$ K that takes into account the presence of biases

A Lagrangian view of transport across the TTL

A. Tzella and B. Legras

Title Page

Abstract

Introduction

Conclusions

References

Tables

Figures

◀

▶

◀

▶

Back

Close

Full Screen / Esc

Printer-friendly Version

Interactive Discussion



in the brightness temperatures (see also Sect. 2.2). It also tests the sensitivity of the results to such biases. No offset is considered for the clear-sky calculation. We thus obtain a set of four CS-TTL ensembles that we label as ALLSKY- ΔT_0 , ALLSKY- ΔT_5 , ALLSKY- ΔT_{-5} and CLRSKY- ΔT_0 .

Figure 2 shows that, when the trajectories are initialised at 100 hPa, the CS-TTL trajectories represent 79–80 % of the entire set of trajectories for all-sky conditions and 72 % for clear-sky conditions. Half of the CS-TTL parcels have encountered a convective source within the last 40 (for $\Delta T = -5$ K) and 51 days (for $\Delta T = 5$ K) for all-sky conditions. For clear-sky conditions, the corresponding time is 75 days. The proportion of CS-TTL trajectories that have encountered a convective source within the last 90 and 200 days is non-negligible for all-sky conditions (17–30 %) and even more so for clear-sky conditions (40 % for simulation CLRSKY- ΔT_0). When the parcels are initialised at 70 hPa, the CS-TTL trajectories represent a smaller proportion of the entire set of trajectories. This is due to the larger distance between the convective sources and the initial level as well as the larger proportion of back trajectories that end up in the extra-tropical stratosphere. Notice that in this case it takes about 40 days for a non-negligible proportion of back trajectories to have encountered a convective source.

2.4 Remaining “free” trajectories

The remaining trajectories have never encountered a cloud at the end of their 200-day back-trajectory. The majority of these “free” trajectories originate from extra-tropical latitudes at the launch surface (see Table 1). In both all-sky and clear-sky conditions, most “free” trajectories end up at higher parts of the stratosphere ($\theta > 400$ K), mostly within the extra-tropics, entrained within the (reverse) Brewer-Dobson circulation. Under all-sky conditions, a small percentage of “free” trajectories end up with $\theta < 400$ K. Conversely, for clear-sky conditions, the proportion of trajectories that are “free” with $\theta < 400$ K, in particular $\theta < 380$ K, is significant. Under these conditions, about half of the “free” trajectories that end up with $\theta < 380$ K are concentrated below the 360 K surface. This is also true in all-sky conditions but the corresponding percentage of “free”

A Lagrangian view of transport across the TTL

A. Tzella and B. Legras

Title Page

Abstract

Introduction

Conclusions

References

Tables

Figures



Back

Close

Full Screen / Esc

Printer-friendly Version

Interactive Discussion



trajectories with $\theta < 380$ K is, in this case, a lot smaller. Thus, the region near the mean tropical C-LZH is a sort of “stagnation” region: As we shall see in Sect. 3.2, air parcels that are detrained within this region can take a long time to exit from it. Equivalently, it takes a long time for back trajectories to encounter a source of convection within this region. For these “free” trajectories, the necessary time exceeds 200 days.

3 Results

We use the CS-TTL trajectory ensembles to identify the source regions for transport of cloud air into the upper TTL. In order to characterise vertical transport across the TTL, we calculate the distribution of times for cloud air to reach its final destination or a particular level for the first time. We determine the distribution of cloud air at its final destination as a function of different range of values for the transport times. Throughout the rest of this paper, we concentrate on those CS-TTL trajectories that are detrained during 2005 (65–66 % of the CS-TTL ensemble for both all-sky and clear-sky conditions).

3.1 Convective sources for transport of cloud air into the stratosphere

3.1.1 Horizontal distributions

For each launch level p , we determine the distribution of convective sources, $\rho(r, t)$, for transport of cloud air into the stratosphere. We do this by calculating the ratio of the number of CS-TTL trajectories that encounter a cloud within the grid-box located at $r = (\lambda, \phi)$, where λ is the longitude and ϕ is the latitude, and time interval $[t, t + \Delta t]$ to a normalisation factor, $N(\phi, \Delta t)$. The value of $N(\phi, \Delta t)$ depends on the latitude ϕ and is given by the product of the grid-box area relative to the area of the tropics, the time-length, Δt , relative to the period concerned (here, 2005) and the total number of CS-TTL trajectories during this period. $N(\phi, \Delta t)$ denotes the expected number of trajectories that would encounter a cloud within a given grid-box, if all regions were

A Lagrangian view of transport across the TTL

A. Tzella and B. Legras

Title Page

Abstract

Introduction

Conclusions

References

Tables

Figures

◀

▶

◀

▶

Back

Close

Full Screen / Esc

Printer-friendly Version

Interactive Discussion



equally likely to contribute to this process (see also Berthet et al., 2007, where a similar normalisation is employed). We choose this normalisation in order to measure the relative importance of different regions for transporting cloud air across the TTL.

Berthet et al. (2007) have previously considered the seasonal variations of the distribution of source regions for transport of air from the boundary layer to the tropopause region. Here, we focus on the density distribution of source regions for transport of cloud air across the TTL and consider both the seasonal ($\Delta t = 3$ months) and daily variations ($\Delta t = 1$ day, whereby each day starts at 00:00 UTC). The daily variations are useful to capture individual convective sources which can thereafter be classified according to their intensity. By employing a daily resolution we thus neglect any variations associated with the diurnal cycle. Each active grid-box must contain enough independent realizations in order to obtain meaningful statistics. We therefore resolve the source distribution on a $5^\circ \times 5^\circ$ longitude/latitude grid.

Figure 3 shows the seasonal variations of the density distribution, $\rho_{100 \text{ hPa}}$, of the locations where trajectories have detrained from clouds and subsequently arrived at 100 hPa. The results are calculated from the ALLSKY- $\Delta T0$ and CLRSKY- $\Delta T0$ trajectory ensembles for boreal winter (DJF), spring (MAM), summer (JJA) and fall seasons (SON). Trajectories are detrained all along 2005. For ALLSKY- $\Delta T0$, a maximum is obtained during the winter and spring seasons (27 % for both seasons). A smaller amount of trajectories are detrained during the summer and autumn seasons (22 % and 23 % respectively – see also Table 2). The corresponding percentages for CLRSKY- $\Delta T0$ are higher by 1 % during boreal winter and by 2 % during boreal spring and autumn seasons. Very similar distributions to the ones shown in Fig. 3 were also found for transport from clouds to the 70 hPa surface (not shown).

The distribution of sources is characterized by strong geographical localization and is consistent with the well-known locations of deep tropical convection (see also e.g., Gettelman et al., 2004; Fueglistaler et al., 2004; Levine et al., 2007). During boreal winter (DJF), the local maxima are over Equatorial Africa, the Southern Asian-Pacific and Southern America. The same three regions are also prominent during the spring

A Lagrangian view of transport across the TTL

A. Tzella and B. Legras

[Title Page](#)[Abstract](#)[Introduction](#)[Conclusions](#)[References](#)[Tables](#)[Figures](#)[◀](#)[▶](#)[◀](#)[▶](#)[Back](#)[Close](#)[Full Screen / Esc](#)[Printer-friendly Version](#)[Interactive Discussion](#)

(MAM) and fall seasons (SON), though other regions, such as the Northern Asian-Pacific and Equatorial America, also become important during this period. During boreal summer, most activity takes place over the Northern Asian-Pacific and Equatorial America.

5 For both ALLSKY- $\Delta T0$ and CLRSKY- $\Delta T0$, we find that the largest contribution of CS-TTL trajectories comes from the Southern Asian-Pacific region (defined by 70° – $200^{\circ} \times -10^{\circ}$ – 20° ; 50% and 44% for all-sky and clear-sky conditions, respectively) while a significant proportion of them has also sources in the Northern Asian-Pacific (bounded by 70° – $200^{\circ} \times 10^{\circ}$ – 35° ; 22% and 27% for all-sky and clear-sky conditions, respectively). A notable contribution comes from Africa (defined by 320° – $20^{\circ} \times -15^{\circ}$ – 20° ; 10% and 13% for all-sky and clear-sky conditions, respectively), followed by Central and Southern America (respectively defined by 250° – $300^{\circ} \times 0^{\circ}$ – 20° ; and 285° – $315^{\circ} \times 0^{\circ}$ – 35° ; 3–6% for both regions and ensembles) – see also Table 3 for ALLSKY- $\Delta T0$ proportions. For both ensembles, the contribution from the Tibetan plateau (defined by 80° – $95^{\circ} \times 30^{\circ}$ – 35°) remains small ($\lesssim 2.5\%$ and $\lesssim 3.6\%$ respectively, of the total and Northern Asian-Pacific boreal summer convective sources). This result is in agreement with recent work by Park et al. (2007); James et al. (2008); Devasthale and Fueglistaler (2010) but does not support previous work by Fu et al. (2006) and Wright et al. (2011) in which the contribution from the Tibetan plateau is found to be important (note that the definition of the Tibetan plateau in Wright et al. (2011) is different to the one employed here and in Fu et al. (2006)). The radiative influence of clouds leads to a noticeable difference (5–6%) in the proportion of trajectories that are detrained by clouds within the Asian-Pacific region. However, this difference is smaller (within $\pm 3\%$) in other regions. Note that the difference in the regional proportions obtained from the ALLSKY- $\Delta T0$, ALLSKY- $\Delta T5$ and ALLSKY- $\Delta T-5$ ensembles is found to be at most 4% (not shown). The same is true for the regional proportions obtained from the ALLSKY- $\Delta T0$ ensemble launched at 100 hPa and 70 hPa.

The distribution of convective sources is highly localized not only in space but also in time. This is evidenced in Fig. 4 in which is plotted the proportion of CS-TTL trajectories

A Lagrangian view of transport across the TTL

A. Tzella and B. Legras

Title Page

Abstract

Introduction

Conclusions

References

Tables

Figures



Back

Close

Full Screen / Esc

Printer-friendly Version

Interactive Discussion



as a function of the day of detrainment. For both ALLSKY- ΔT_0 and CLRSKY- ΔT_0 ensembles, this proportion is characterized by highly variable daily fluctuations, with this variability being larger under clear-sky conditions.

3.1.2 Localization of the horizontal distributions

5 The spatio-temporal localisation of the daily-varying $\rho(r,t)$ can be analysed by considering the fraction of horizontal locations and times that have a density distribution whose value exceeds a given threshold, ϱ . More precisely, we define:

$$A(\varrho) = \frac{1}{\Omega} \int_T dt \int_{\sigma} dr \mathcal{J}_{\varrho}(r,t), \quad (2a)$$

where \mathcal{J}_{ϱ} is the indicator function:

$$10 \mathcal{J}_{\varrho}(r,t) = \begin{cases} 1, & \text{if } \rho(r,t) \geq \varrho, \\ 0, & \text{otherwise,} \end{cases} \quad (2b)$$

and Ω denotes the total space-time volume. Its value is given by $\Omega = \int_T dt \int_{\sigma} dr \mathcal{J}_0(r,t)$, where σ denotes the region in which the sources of convection are resolved (here, the tropics) and T the time period concerned (here, the year 2005). It follows that $A(0) = 1$.

Thus, by considering increasingly large values of ϱ , we obtain the fraction of space-time volume associated with increasingly intense sources. The fraction of trajectories associated with $A(\varrho)$ is given by

$$15 P(\varrho) = \int \mathcal{J}_{\varrho}(r,t) \rho(r,t) dr dt. \quad (2c)$$

By definition $A(\varrho)$ is a monotonically decreasing function of ϱ and thus there exists a unique inverse, $\varrho(A)$. Employing this inverse, we compose $P_{\varrho}(A) \equiv (P \circ \varrho)(A)$. A function of the space-time volume, $P_{\varrho}(A)$ measures how localized the source distribution is. It can be shown that $P_{\varrho}(A)$ is a monotonically increasing function of A with $\lim_{A \rightarrow 0} P_{\varrho} = 0$ and $\lim_{A \rightarrow 1} P_{\varrho} = 1$. The value of A for which $P_{\varrho}(A) = 0.5$ or 0.99 indicate the degree of

A Lagrangian view of transport across the TTL

A. Tzella and B. Legras

Title Page

Abstract

Introduction

Conclusions

References

Tables

Figures

◀

▶

◀

▶

Back

Close

Full Screen / Esc

Printer-friendly Version

Interactive Discussion



localization of the distribution. The smaller their values are, the more localized is the source distribution.

We employ $P_{\rho}(A)$ to measure how localised $\rho_{100 \text{ hPa}}$ is, as this varies daily. For comparison, $P_{\rho}(A)$ is calculated for all four CS-TTL ensembles. Figure 5a shows that a very small (0.5–2 %) proportion of Ω accounts for half of the trajectories (associated with the most intense sources) and 3–8 % of Ω accounts for nearly all (99 %) of the CS-TTL trajectories. Note that the corresponding proportions are considerably larger for the distribution $\tilde{\rho}_{100 \text{ hPa}}$ obtained by randomly distributing the same number of trajectories uniformly in both space and time.

The source distribution that is most localised is the one obtained under clear-sky conditions. The least localised distribution corresponds to the one obtained under all-sky conditions, having taken into account a thermal bias of $\Delta T = -5$. This is consistent with the fact that the C-LZH is, on average, higher than the A-LZH, leading to a smaller proportion of cloud air at higher parts of the TTL. Conversely, under all-sky conditions, when the thermal bias becomes progressively smaller (from $\Delta T = 5$ to $\Delta T = 0$ and then $\Delta T = -5$), the top of clouds become progressively raised, leading to a larger proportion of cloud air in the upper TTL.

We now employ $P_{\rho}(A)$ to measure how the structure of $\rho_{100 \text{ hPa}}$ varies with the season. In this case, Ω denotes the total space-time volume during a particular season. Interestingly, the degree of source localization varies very little with the season (see Fig. 5b calculated from the ALLSKY- $\Delta T 0$ ensemble). This is consistent with the observed lack of seasonal differences in the proportion of CS-TTL parcels (see Table 2).

3.1.3 Cloud top brightness temperatures

The cumulative distributions of the cloud top brightness temperatures (BT) of those clouds encountered by the CS-TTL parcels are shown in Fig. 6a for the four trajectories ensembles, launched at 100 hPa (the same results are obtained for simulations launched at 70 hPa). Nearly all (90 %) of the CS-TTL parcels have detrained from very deep clouds (with $BT \leq 220 \text{ K}$ and $BT \leq 203 \text{ K}$ for transport under all-sky and clear-sky

A Lagrangian view of transport across the TTL

A. Tzella and B. Legras

Title Page

Abstract

Introduction

Conclusions

References

Tables

Figures

◀

▶

◀

▶

Back

Close

Full Screen / Esc

Printer-friendly Version

Interactive Discussion



conditions, respectively). As expected, the air parcels sample the deepest convective sources more efficiently in clear-sky than in all-sky conditions. This is because in all-sky conditions, the CS-TTL trajectories can be detrained from convective sources that have a broader range of brightness temperatures than in clear-sky conditions (recall that the mean A-LZH is lower than the mean C-LZH).

No seasonal variations are observed in the BT cumulative distributions (see Fig. 6b). However, some regional variations are present (see Fig. 6a) with the deepest convective sources located within the region of Africa, followed by the region of Southern and Central America (see also Table 3). These regional characteristics are consistent with previous observations that find that the deepest convective events occur predominantly over land, particularly above the region of Africa (see e.g., Liu and Zipser, 2005).

3.1.4 Localization of the horizontal distributions among increasingly deep clouds

It is interesting to construct a measure of how $\rho(r,t)$ is partitioned among the space occupied by clouds. For it is not clear that all sufficiently deep clouds will participate in the same way in troposphere-to-stratosphere transport. In particular, large-scale horizontal advection can transport cloud air that is detrained within a certain region into other regions where the LZH has a higher potential temperature, and subsequently may subside back into the troposphere (see also discussion in Devasthale and Fueglistaler, 2010). It can also be that the fast upward motion associated with cirrus clouds only occurs around a selected number of deep convective clouds. This is because cirrus clouds may either not be present or cloud air may subside due to the radiative cooling associated with that part of the cirrus that is situated directly above deep convective clouds (see Hartmann et al., 2001). Both these mechanisms could be significant in controlling how influential a convective source will be in transporting cloud air into the stratosphere.

To measure how localized $\rho(r,t)$ is within the space occupied by clouds, we employ $P_{q|T^*}(A)$, a variant of $P_q(A)$, introduced in Sect. 3.1.2, that describes how localised the

A Lagrangian view of transport across the TTL

A. Tzella and B. Legras

[Title Page](#)[Abstract](#)[Introduction](#)[Conclusions](#)[References](#)[Tables](#)[Figures](#)[Back](#)[Close](#)[Full Screen / Esc](#)[Printer-friendly Version](#)[Interactive Discussion](#)

source distribution is in Ω_{T^*} , where Ω_{T^*} is defined as the total space-time volume with brightness temperature, $BT \leq T^*$. We can thus define \mathcal{A} as in Eq. (2) but this time in terms of Ω_{T^*} and $\mathcal{J}_{\varrho|T^*}$ where

$$\mathcal{J}_{\varrho|T^*}(r, t) = \begin{cases} 1, & \text{if } \rho(r, t) \geq \varrho \text{ and } BT(r, t) \leq T^*, \\ 0, & \text{otherwise.} \end{cases} \quad (3)$$

$P_{\varrho|T^*}(\mathcal{A})$ thus measures how transport into the stratosphere is partitioned among convective sources that reach similar depths in the troposphere.

In order to calculate $P_{\varrho|T^*}(\mathcal{A})$, we resolve the sources on the same grid as the BT measurements (see Sect. 2.2). This resolution is of course too high for $P_{\varrho|T^*}(\mathcal{A})$ to converge to an invariant form that is insensitive to the frequency at which the trajectories are launched (note that this is not the case for $P_{\varrho}(\mathcal{A})$, shown in Fig. 5, which unlike $P_{\varrho|T^*}(\mathcal{A})$, is based on a significantly lower resolution in both space and time for the source distribution). It is nevertheless possible to obtain an understanding of how transport across the TTL is partitioned among the different convective sources. It suffices to consider the departure of $P_{\varrho|T^*}(\mathcal{A})$ from a reference $P_{\varrho|T^*}(\mathcal{A})$, obtained by uniformly randomly distributing the same number of detrained parcels among horizontal locations with $BT \leq T^*$.

We consider three different BT threshold values, $T^* = 215, 200$ and 185 K, and calculate $P_{\varrho|T^*}(\mathcal{A})$ from the ALLSKY- $\Delta T0$ ensemble launched at 100 hPa. The results are shown in Fig. 7. As expected, the deeper the convective sources (the smaller the value of T^*), the more efficiently they are sampled. At the same time, $P_{\varrho|T^*}(\mathcal{A})$ significantly differs from the mean $P_{\varrho|T^*}(\mathcal{A})$ obtained from 1000 realisations. In particular, the entirety of the CS-TTL parcels sample a proportion of the horizontal locations that would be sampled if the parcels were randomly distributed among them (54, 70 and 76 %, respectively for $T^* = 215, 200$ and 185 K). This proportion becomes considerably smaller when half of the CS-TTL parcels (associated with the most intense sources) are considered (17, 50 and 63 %, respectively for $T^* = 215, 200$ and 185 K). The large differences between $P_{\varrho|T^*}(\mathcal{A})$ and $P_{\varrho|T^*}(\mathcal{A})$ suggest that the transport of cloud air into

A Lagrangian view of transport across the TTL

A. Tzella and B. Legras

Title Page

Abstract

Introduction

Conclusions

References

Tables

Figures

◀

▶

◀

▶

Back

Close

Full Screen / Esc

Printer-friendly Version

Interactive Discussion



the stratosphere is not equally partitioned among clouds of similar cloud top BT. At the same time, these differences decrease with increasingly deep sources (i.e., when T^* decreases from 215 to 185 K).

Note that in clear-sky conditions, the difference between $P_{\varrho|T^*}(A)$ and $P_{\varrho|T^*}(A)$ is larger (not shown). This is because in these conditions, the number of CS-TTL parcels that are detrained from very deep convection is larger than in all-sky conditions (see Fig. 6). Therefore, the corresponding statistics are closer to their invariant form attained for sufficiently large number of parcels.

3.1.5 Vertical distributions

The distributions of the potential temperatures at which the CS-TTL trajectories encounter a cloud are shown in Fig. 8a for the four trajectory ensembles, launched at 100 hPa (nearly identical results are obtained for trajectories launched at 70 hPa). Under all-sky conditions, the distributions of these potential temperatures are mainly confined between 350 and 360 K. For all ΔT , no encounters of clouds take place below 340 K (i.e., all encounters take place above or near the mean level of maximum convective outflow). For $\Delta T = 0$, 10% of the encounters occur above 360 K (the corresponding percentage for $\Delta T = 5$ K and -5 K is 5 and 20 %, respectively) while only 4 % occur above 365 K (the corresponding percentage for $\Delta T = 5$ K and -5 K is 1 and 10 %, respectively). Under clear-sky conditions, the corresponding potential temperature distribution is narrower, with no cloud encounters taking place below 352 K while only 5 % occurring above 366 K.

In the absence of thermal biases (i.e., $\Delta T = 0$), the mean potential temperature is equal to the mean LZH in both all-sky and clear-sky cases (see also Table 4). When we consider a thermal bias of $\Delta T = -5$ K (equivalent to raising cloud heights), the average is displaced by 2 K to a larger value of potential temperature. Conversely, a displacement of 1 K to a lower value is obtained when we consider a thermal bias of $\Delta T = 5$ K (equivalent to lowering cloud heights). Near the tropopause, $\Delta\theta \approx -2\Delta T$. Thus, there is no direct relation between the mean displacement in potential temperature and the

A Lagrangian view of transport across the TTL

A. Tzella and B. Legras

Title Page

Abstract

Introduction

Conclusions

References

Tables

Figures

◀

▶

◀

▶

Back

Close

Full Screen / Esc

Printer-friendly Version

Interactive Discussion



mean displacement in the cloud top height.

Figure 8(b) shows the seasonal variations of the potential temperature distributions obtained from the ALLSKY- $\Delta 70$ ensemble, launched at 100 hPa. The potential temperatures are nearly identically distributed for CS-TTL parcels detrained during the boreal winter and spring season; during the autumn season, the distribution is similar but shifted to slightly lower values (see also Table 2). The main difference occurs for CS-TTL parcels detrained during the summer. In this case, the parcels' potential temperatures appear to have a distribution that has two peaks, the first peak being located at about 352 K and the second one at 358 K.

A similar behaviour, albeit weaker, is observed for parcels detrained in the Northern Asian-Pacific region which is mainly active during the summer season (see Fig. 8c). We find that the first peak is mainly due to detrainment over the ocean while the second peak is due to detrainment over the land part of the Northern Asian-Pacific that can take place at latitudes higher than 20° N. An interpretation of this fact is that poleward of 20° N and 20° S, both the C-LZH and the A-LZH are sloping upward in potential temperature, with this effect being most pronounced for the A-LZH (see Fig. 2 in Fueglistaler et al., 2009b). Hence, at these higher latitudes, convection must reach higher to contribute to upward moving air in the TTL.

Note that the above land-ocean differences are not reflected in the brightness temperatures of the corresponding convective sources. More generally, there is no direct relation between the mean potential temperature of cloud encounters and the mean brightness temperature of the corresponding convective sources (e.g. although the deepest convective sources occur more frequently in the region of Africa, the average height of cloud encounter within this region is not significantly different to the average height of cloud encounter in other regions, such as the Southern Asian-Pacific region, in which, in general, convection does not reach as high (see also Sect. 3.1.3)).

A Lagrangian view of transport across the TTL

A. Tzella and B. Legras

Title Page

Abstract

Introduction

Conclusions

References

Tables

Figures



Back

Close

Full Screen / Esc

Printer-friendly Version

Interactive Discussion



3.2 Timescales for transport of cloud air across the TTL and into the lower stratosphere

3.2.1 First-entry times

We now focus on the time it takes for CS-TTL parcels to first enter (in forward time) the upper TTL and the stratospheric “overworld”. Figure 9a shows the histograms of times to first reach the 370 K and 380 K surfaces for the four trajectory ensembles, launched at 100 hPa. Similar histograms are obtained for trajectories launched at 70 hPa (not shown). In both all-sky and clear-sky cases, the histograms are broad and skewed, decaying exponentially at large times.

The histograms obtained under all-sky conditions are characterized by a pronounced peak, located at approximately 15 days, that is largely unaffected by a variable offset, ΔT . Note that the location of the peak is consistent with the estimated time that Corti et al. (2006) obtained for cloud air to first reach the 370 K surface, provided it stays inside a cirrus for most of the time. Conversely, the corresponding histogram obtained for clear-sky conditions is notably broader, with a slower decay rate at large times.

The average time to first reach the 370 K surface is, depending on the value of ΔT , between 23 and 31 days for all-sky conditions and 54 days for clear-sky. The corresponding time for the 380 K surface is between 33 and 44 days for all-sky conditions and 64 for clear-sky (see also Table 5). It is thus clear that the radiative heating associated with clouds significantly accelerates transport across the TTL.

The radiative influence of clouds on transport across the TTL is mainly confined to the region below the 360 K surface. This is evidenced in Fig. 9b in which the histograms of times to cross the 360–370 K and 360–380 K layers are shown to be similar in all-sky and clear-sky conditions (note that to obtain these histograms we ignore those CS-TTL parcels that never go below 360 K).

At the same time, these histograms are considerably narrower than the histograms shown in Fig. 9a. The large width of the latter are due the large dispersion in the times to exit the region below 360 K. The mean exit time is 15 days for all-sky conditions and

A Lagrangian view of transport across the TTL

A. Tzella and B. Legras

Title Page

Abstract

Introduction

Conclusions

References

Tables

Figures



Back

Close

Full Screen / Esc

Printer-friendly Version

Interactive Discussion



$\Delta T = 0$ and 42 days for clear-sky conditions. The first mean is consistent with simple estimates such as those shown in Fig. 1b obtained for $\theta_0 \approx 355$ K (recall that in all-sky conditions, the mean potential temperature at which parcels detrain is 354 K). The second mean cannot be explained using these sort of estimates.

The large width of the first-entry time histograms are a result of the combined effect of the radiative heating rates and horizontal motion around the LZH (whose mean level in the tropics coincides with the mean potential temperature at which the CS-TTL parcels are detrained in both clear and all sky conditions). Horizontal motion can lead air parcels to alternate regions situated just below and above the LZH (equivalent to alternate regions of negative and positive heating rates), so that the air parcels respectively descend and rise. The corresponding fluctuations in the vertical velocities impede the immediate ascent of a number of air parcels to higher altitudes. This is particularly true for clear-sky conditions: Without the radiative influence of cirrus clouds, the fluctuations in the vertical velocities are of smaller amplitude than in all-sky conditions. As a result, parcels that are detrained below the mean C-LZH have less possibilities to escape to regions, sufficiently above the mean C-LZH, where the mean flow is strong. When this happens, the mean flow regains control over their vertical transport and the dispersion in the vertical motion becomes smaller. This indeed explains why the histograms in Fig. 9b are narrower than the histograms in Fig. 9a. It also explains the large number of “free” trajectories (i.e., trajectories that have not detrained from a convective source) that are found in this region, particularly for clear-sky conditions (see Sect. 2.4). Note that the possibility of long trapping times near the C-LZH has previously been reported in an idealized study by Sherwood and Dessler (2003) in which the mean flow is represented by the linearized, clear-sky mean tropical radiative heating rate profile while the dispersive effect of horizontal advection on the vertical motion is represented by a diffusive process.

A Lagrangian view of transport across the TTL

A. Tzella and B. Legras

Title Page

Abstract

Introduction

Conclusions

References

Tables

Figures

◀

▶

◀

▶

Back

Close

Full Screen / Esc

Printer-friendly Version

Interactive Discussion



3.2.2 Transit-times

The distribution of transit-times between detrainment and launch are shown in Fig. 9c for air parcels initially at 100 hPa (note that the cumulative histograms shown in Fig. 2 correspond to a larger set of CS-TTL trajectories that also detrain during some of 2004 and 2006). The longer time necessary for the air parcels to reach their final destinations (in forward time) on the launch surface at higher latitudes is responsible for the larger width of the histograms (compare with the histograms shown in Fig. 9a). Note that once again, the radiative heating associated with cirrus clouds are behind the pronounced peaks observed in Fig. 9c. The mean transit-time is between 53 and 64 days for all-sky conditions and 83 days for clear-sky (see also Table 4).

Figure 10 shows that the above mentioned histograms do not depend strongly on seasonal or regional characteristics (see Fig. 10). Any differences are present for the early transport of air parcels (see insets in Fig. 10a and b). During boreal summer, air parcels are relatively slower in reaching the 100 hPa surface: only 12 % of cloud air detrained during that season reaches its final destination on the 100 hPa surface within 20 days which is about half the amount obtained during the other seasons (see Fig. 10a). Similarly, air parcels detrained within the Northern Asian-Pacific region (that is mainly active during boreal summer), particularly those detrained over land, are slow to reach their final destination on the 100 hPa surface: 15 % of cloud air arrives within 20 days. This is to be contrasted with 25 % of air parcels detrained in the Southern Asian-Pacific region in which early transport is the fastest (see Fig. 10b). These differences are despite the higher potential temperatures at which air parcels detrain during both boreal summer and the Northern Asian-Pacific region (see Fig. 8). Their slow ascent into the upper TTL is the combined result of the monsoon anticyclone that dominates the large-scale boreal summer circulation within this region and the smaller, on average, tropical radiative heating rates above approximately 365 K in comparison to the other seasons (not shown).

A Lagrangian view of transport across the TTL

A. Tzella and B. Legras

Title Page

Abstract

Introduction

Conclusions

References

Tables

Figures



Back

Close

Full Screen / Esc

Printer-friendly Version

Interactive Discussion



3.3 Distribution of cloud air in the lower stratosphere

The extensive large-scale horizontal motion that takes place within the TTL (Holton and Gettelman, 2001; Fueglistaler et al., 2004; Bonazzola and Haynes, 2004) ensures that, at the lower stratosphere (at about 100 hPa), air of convective origin is, in general, well-mixed in the longitude. The distributions, $\chi(r, \tau)$, of the final locations (in forward time) of the CS-TTL trajectories differ according to the range of values of their transit-times.

We determine $\chi(r, \tau)$ by calculating the ratio of the number of CS-TTL trajectories, detrained during a certain season, located within the grid-box at r and transit-times within $[\tau, \tau + \Delta\tau]$ to a normalization factor, $\tilde{N}(\phi, \Delta\tau)$. We choose a similar normalization to the one employed for $\rho(r, t)$ in Sect. 3.1.1: The value of $\tilde{N}(\phi, \Delta\tau)$ depends on the latitude ϕ and is given by the product of the grid-box area relative to the area of launch surface (50° S, 50° N), the transit-time length, $\Delta\tau$, relative to the maximum possible transit-time (here, 200 days) and the total number of CS-TTL trajectories detrained during the season concerned. $\tilde{N}(\phi, \Delta\tau)$ denotes the expected number of CS-TTL trajectories within a grid-box if all regions in the launch surface were equally likely to contribute to transport across the TTL with the last encounter with a convective source being uniformly distributed within the period concerned (here, 200 days).

Figure 11 shows $\chi_{100\text{hPa}}$ calculated from the ALLSKY- $\Delta T0$ trajectory ensemble, launched at 100 hPa, for trajectories detrained during boreal winter (DJF) and summer (JJA). For both seasons we can identify three spatial regimes for $\chi(r, \tau)$. For small transit times ($\tau \lesssim 15$ days), the distribution of the CS-TTL parcels at the 100 hPa surface are localized, with the local maxima located at or near the convective source regions (see also Fig. 3). This regime corresponds to about a tenth of the CS-TTL parcels (13 and 7% for parcels detrained during DJF and JJA, respectively). For intermediate transit-times ($\tau \approx 15\text{--}60$ days), the distributions of the CS-TTL parcels are quasi-homogeneous within nearly the whole 100 hPa surface between the tropics (30° S, 30° N). Notice the appearance of a local maximum in the region in which the monsoon anticyclone dominates during boreal summer. This regime corresponds to

A Lagrangian view of transport across the TTL

A. Tzella and B. Legras

Title Page

Abstract

Introduction

Conclusions

References

Tables

Figures

◀

▶

◀

▶

Back

Close

Full Screen / Esc

Printer-friendly Version

Interactive Discussion



about half of the CS-TTL parcels (49 and 52 % for parcels detrained during DJF and JJA, respectively). For large transit-times ($\tau \approx 60\text{--}200$ days), the distributions of the CS-TTL parcels are mostly present in the extra-tropics, within which they are quasi-homogeneous. This regime corresponds to about four tenths of the CS-TTL parcels (38 and 41 % respectively, for parcels detrained during DJF and JJA). The transition between the last two regimes may also be observed in the latitudinal distributions of the CS-TTL trajectories shown on the right of Fig. 11 for each of the three range of values for the transit-times.

A similar set of spatial regimes characterises $\chi_{100\text{ hPa}}$ obtained under clear-sky conditions (not shown). However in these conditions, the amount of air associated with each regime is different to the corresponding amount obtained under all-sky conditions. For example, the amount of cloud air that is detrained within the last 15 days is about a half or a third (4 % for both DJF and JJA) of the corresponding amount obtained in all-sky conditions.

4 Conclusions

Previous considerations (Corti et al., 2005, 2006) have suggested that the radiative heating from cirrus clouds could play an important role in transporting air across the C-LZH – a barrier for vertical transport which must be overcome for air of convective origin to eventually reach the upper TTL and lower stratosphere. In this study, we have employed a novel Lagrangian approach which combines a large number of backward diabatic trajectory calculations (in both clear-sky and all-sky conditions) with global fields of brightness temperatures in order to analyse the combined effect of cloud heating and large-scale horizontal motion on the transport of air across the TTL. The result is a quantitative picture of the seasonal and regional characteristics of convective sources and times for transport of air into the upper TTL and lower stratosphere.

We have shown that the lower, on average, level of A-LZH (in which the radiative heating of clouds is included) and the larger, in general, heating rates, both associated

A Lagrangian view of transport across the TTL

A. Tzella and B. Legras

Title Page

Abstract

Introduction

Conclusions

References

Tables

Figures

◀

▶

◀

▶

Back

Close

Full Screen / Esc

Printer-friendly Version

Interactive Discussion



Secondly, the use of radiative heating rates to represent vertical motion out of convection means that the descending trajectory motions associated with clear-sky regions between deep convective clouds are represented. It would be interesting to compare our results with corresponding results obtained in other Lagrangian models such as the one employed in Pisso et al. (2010) in which a convective parameterisation is taken into account and found to have a large impact on the ozone depletion potentials for VSLs.

There are a number of limitations to the results presented in this study that are already described. The most important limitation concerns the realism of the radiative heating rates in the ERA-Interim re-analysis dataset. As already noted, uncertainty in their values arises mostly due the influence of clouds. Despite this uncertainty, we believe that motion near the A-LZH will continue to depend on its fluctuating structure as the accuracy in the values of the radiative heating rates increases. Further work will require the comparison with radiative calculations performed using real distribution of clouds, as diagnosed, e.g. by CloudSat/CALIPSO (Sassen et al., 2008; Martins et al., 2011).

Acknowledgements. The authors thank G. Berthet, M. Bolot, J-P. Duvel, S. Fueglistaler, P. H. Haynes, S. Y. Liu and T-Y. Koh for useful discussions. The results were obtained using ERA-Interim data, provided by the ECMWF, and the CLAUS archive, held at the British Atmospheric Data Centre (BADC) and produced using source data from the ISCCP that are made available at the NASA Langley Atmospheric Sciences Data Center (LASDC). A. Tzella acknowledges financial support from the Marie Curie Individual fellowship HydraMitra No. 221827.



The publication of this article is financed by CNRS-INSU.

18188

ACPD

11, 18161–18209, 2011

A Lagrangian view of transport across the TTL

A. Tzella and B. Legras

Title Page

Abstract

Introduction

Conclusions

References

Tables

Figures

⏪

⏩

◀

▶

Back

Close

Full Screen / Esc

Printer-friendly Version

Interactive Discussion



References

- Berthet, G., Esler, J. G., and Haynes, P. H.: A Lagrangian perspective of the tropopause and the ventilation of the lowermost stratosphere, *J. Geophys. Res.*, 112, D18102, doi:10.1029/2006JD008295, 2007. 18174
- 5 Bonazzola, M. and Haynes, P. H.: A trajectory-based study of the tropical tropopause region, *J. Geophys. Res.*, 109, D20112, doi:10.1029/2003JD004356, 2004. 18164, 18185
- Corti, T., Lup, B. P., Peter, T., Vömel, H., and Fu, Q.: Mean radiative energy balance and vertical mass fluxes in the equatorial upper troposphere and lower stratosphere, *Geophys. Res. Lett.*, 32, L06 802, doi:10.1029/2004GL021889, 2005. 18164, 18186
- 10 Corti, T., Luo, B. P., Fu, Q., Vömel, H., and Peter, T.: The impact of cirrus clouds on tropical troposphere-to-stratosphere transport, *Atmos. Chem. Phys.*, 6, 2539–2547, doi:10.5194/acp-6-2539-2006, 2006. 18164, 18182, 18186, 18187
- Dee, D. P., Uppala, S. M., Simmons, A. J., Berrisford, P., Poli, P., Kobayashi, S., Andrae, U., Balmaseda, M. A., Balsamo, G., Bauer, P., Bechtold, P., Beljaars, A. C. M., van de Berg, L., Bidlot, J., Bormann, N., Delsol, C., Dragani, R., Fuentes, M., Geer, A. J., Haimberger, L., Healy, S. B., Hersbach, H., Hólm, E. V., Isaksen, L., Kållberg, P., Köhler, M., Matricardi, M., McNally, A. P., Monge-Sanz, B. M., Morcrette, J.-J., Park, B.-K., Peubey, C., de Rosnay, P., Tavolato, C., Thépaut, J.-N., and Vitart, F.: The ERA-Interim reanalysis: configuration and performance of the data assimilation system, *Q. J. Roy. Meteor. Soc.*, 137, 553–597, doi:10.1002/qj.828, 2011. 18166
- 20 Devasthale, A. and Fueglistaler, S.: A climatological perspective of deep convection penetrating the TTL during the Indian summer monsoon from the AVHRR and MODIS instruments, *Atmos. Chem. Phys.*, 10, 4573–4582, doi:10.5194/acp-10-4573-2010, 2010. 18175, 18178
- Folkins, I., Lowenstein, M., Podolske, J. R., Oltmans, S. J., and Proffitt, M.: A barrier to vertical mixing at 14 km in the tropics: Evidence from ozonesondes and aircraft measurements, *J. Geophys. Res.*, 104, 22095–22102, doi:10.1029/1999JD900404, 1999. 18163
- 25 Fu, Q., Hu, Y., and Yang, Q.: Identifying the top of the tropical tropopause layer from vertical mass flux analysis and CALIPSO lidar cloud observations, *Geophys. Res. Lett.*, 34, L14813, doi:10.1029/2007GL030099, 2007. 18163, 18170
- 30 Fu, Y., Liu, G., Wu, G., Yu, R., Xu, Y., Wang, Y., Li, R., and Liu, Q.: Tower mast of pre-precipitation over the Central Tibetan Plateau summer, *Geophys. Res. Lett.*, 33, L05802, doi:10.1029/2005GL024713, 2006. 18175

A Lagrangian view of transport across the TTL

A. Tzella and B. Legras

Title Page

Abstract

Introduction

Conclusions

References

Tables

Figures

◀

▶

◀

▶

Back

Close

Full Screen / Esc

Printer-friendly Version

Interactive Discussion



Fueglistaler, S., Wernli, H., and Peter, T.: Tropical troposphere-to-stratosphere transport inferred from trajectory calculations, *J. Geophys. Res.*, 109, D03108, doi:10.1029/2003JD004069, 2004. 18164, 18174, 18185

Fueglistaler, S., Bonazzola, M., Haynes, P. H., and Peter, T.: Stratospheric water vapor predicted from the Lagrangian temperature history of air entering the stratosphere in the tropics, *J. Geophys. Res.*, 110, D08107, doi:10.1029/2004JD005516, 2005. 18170

Fueglistaler, S., Dessler, A. E., Dunkerton, T. J., Folkins, I., Fu, Q., and Mote, P. W.: Tropical tropopause layer, *Rev. Geophys.*, 47, RG1004, doi:10.1029/2008RG000267, 2009a. 18163

Fueglistaler, S., Legras, B., Beljaars, A., Morcrette, J.-J., Simmons, A., Tompkins, A. M., and Uppala, S.: The diabatic heat budget of the upper troposphere and lower/mid stratosphere in ECMWF reanalyses, *Q. J. Roy. Meteor. Soc.*, 135, 21–37, doi:10.1002/qj.361, 2009b. 18167, 18171, 18181

Gettelman, A. and de Forster, P. M.: Definition and climatology of the tropical tropopause layer, *J. Meteorol. Soc. Jpn.*, 80, 911–924, 2002. 18163

Gettelman, A., de Forster, P. M., Fujiwara, M., Fu, Q., Vömel, H., Gohar, L. K., Johanson, C., and Ammerman, M.: Radiation balance of the tropical tropopause layer, *J. Geophys. Res.*, 109, D07103, doi:10.1029/2003JD004190, 2004. 18163, 18174

Hartmann, D. L., Holton, J. R., and Fu, Q.: The heat balance of the tropical tropopause, cirrus, and stratospheric dehydration, *Geophys. Res. Lett.*, 28, 1969–1972, doi:10.1029/2000GL012833, 2001. 18178

Highwood, E. J. and Hoskins, B. J.: The tropical tropopause, *Q. J. Roy. Meteorol. Soc.*, 124, 1579–1604, doi:10.1002/qj.49712454911, 1998. 18163

Hodges, K. D., Chappell, W., Robinson, G. J., and Yang, G.: An improved algorithm for generating global window brightness temperatures from multiple satellite infrared imagery, *J. Atmos. Ocean. Tech.*, 17, 1296–1312, doi:10.1175/1520-0426(2000)017<1296:AIAFGG>2.0.CO;2, 2000. 18169

Holton, J. R. and Gettelman, A.: Horizontal transport and the dehydration of the stratosphere, *Geophys. Res. Lett.*, 28, 2799–2802, doi:10.1029/2001GL013148, 2001. 18164, 18185

Holton, J. R., Haynes, P. H., McIntyre, M. E., Douglass, A. R., Rood, R. B., and Pfister, L.: Stratosphere-troposphere exchange, *Rev. Geophys.*, 33, 403–439, doi:10.1029/95RG02097, 1995. 18163

James, R., Bonazzola, M., Legras, B., Surbled, K., and Fueglistaler, S.: Water vapor transport and dehydration above convective outflow during Asian monsoon, *Geophys. Res. Lett.*, 35,

A Lagrangian view of transport across the TTL

A. Tzella and B. Legras

Title Page

Abstract

Introduction

Conclusions

References

Tables

Figures

◀

▶

◀

▶

Back

Close

Full Screen / Esc

Printer-friendly Version

Interactive Discussion



A Lagrangian view of transport across the TTL

A. Tzella and B. Legras

Title Page

Abstract

Introduction

Conclusions

References

Tables

Figures

◀

▶

◀

▶

Back

Close

Full Screen / Esc

Printer-friendly Version

Interactive Discussion



L20810, doi:10.1029/2008GL035441, 2008. 18170, 18171, 18175

Levine, J. G., Braesicke, P., Harris, N. R. P., Savage, N. H., and Pyle, J. A.: Pathways and timescales for troposphere-to-stratosphere transport via the tropical tropopause layer and their relevance for very short lived substances, *J. Geophys. Res.*, 112, D04308, doi:10.1029/2005JD006940, 2007. 18174

Liu, C. and Zipser, E. J.: Global distribution of convection penetrating the tropical tropopause, *J. Geophys. Res.*, 110, D23104, doi:10.1029/2005JD006063, 2005. 18163, 18170, 18178

Liu, Y. S., Fueglistaler, S., and Haynes, P. H.: The advection-condensation paradigm for stratospheric water vapour, *J. Geophys. Res.*, 115, D24307, doi:10.1029/2010JD014352, 2010. 18166, 18170

Martins, E., Noel, V., and Chepfer, H.: Properties of cirrus and subvisible cirrus from nighttime Cloud-Aerosol Lidar with Orthogonal Polarization (CALIOP), related to atmospheric dynamics and water vapor, *J. Geophys. Res.*, 116, D02208, doi:10.1029/2010JD014519, 2011. 18164, 18188

Massie, S., Gettelman, A., Randel, W., and Baumgardner, D.: Distribution of tropical cirrus in relation to convection, *J. Geophys. Res.*, 107(D21), 4591, doi:10.1029/2001JD001293, 2002. 18164

Nawrath, S.: Water vapor in the tropical upper troposphere: on the influence of deep convection, Ph.D. thesis, Universität Köln, Germany, 2002. 18170

Park, S., Jiménez, R., Daube, B. C., Pfister, L., Conway, T. J., Gottlieb, E. W., Chow, V. Y., Curran, D. J., Matross, D. M., Bright, A., Atlas, E. L., Bui, T. P., Gao, R.-S., Twohy, C. H., and Wofsy, S. C.: The CO₂ tracer clock for the Tropical Tropopause Layer, *Atmos. Chem. Phys.*, 7, 3989–4000, doi:10.5194/acp-7-3989-2007, 2007. 18175

Pisso, I. and Legras, B.: Turbulent vertical diffusivity in the sub-tropical stratosphere, *Atmos. Chem. Phys.*, 8, 697–707, doi:10.5194/acp-8-697-2008, 2008. 18166

Pisso, I., Haynes, P. H., and Law, K. S.: Emission location dependent ozone depletion potentials for very short-lived halogenated species, *Atmos. Chem. Phys.*, 10, 12025–12036, doi:10.5194/acp-10-12025-2010, 2010. 18188

Ploeger, F., Konopka, P., Günther, G., Grooss, J.-U., and Müller, R.: Impact of the vertical velocity scheme on modeling transport in the tropical tropopause layer, *J. Geophys. Res.*, 115, D03301, doi:10.1029/2009JD012023, 2010. 18168

Sassen, K., Wang, Z., and Liu, D.: Global distribution of cirrus clouds from CloudSat/Cloud-Aerosol Lidar and Infrared Pathfinder Satellite Observations (CALIPSO) measurements, *J.*

- Geophys. Res., 113, D00A12, doi:10.1029/2008JD009972, 2008. 18188
- Schiller, C., Grooß, J.-U., Konopka, P., Plöger, F., Silva dos Santos, F. H., and Spelten, N.: Hydration and dehydration at the tropical tropopause, *Atmos. Chem. Phys.*, 9, 9647–9660, doi:10.5194/acp-9-9647-2009, 2009. 18170
- 5 Schoeberl, M. R., Douglass, A. R., Zhu, Z., and Pawson, S.: A comparison of the lower stratospheric age spectra derived from a general circulation model and two data assimilation systems, *J. Geophys. Res.*, 108, 4113, doi:10.1029/2002JD002652, 2003. 18166
- Sherwood, S. C. and Dessler, A. E.: Convective Mixing near the Tropical Tropopause: insights from seasonal variations, *J. Atmos. Sci.*, 60, 2674–2685, doi:10.1175/1520-0469(2003)060<2674:CMNTTT>2.0.CO;2, 2003. 18183
- 10 Sherwood, S. C., Chae, J.-H., Minnis, P., and McGill, M.: Underestimation of deep convective cloud tops by thermal imagery, *Geophys. Res. Lett.*, 31, L11102, doi:10.1029/2004GL019699, 2004. 18169
- Stohl, A., Wernli, H., James, P., Bourqui, M., Forster, C., Liniger, M. A., Seibert, P., and Sprenger, M.: A new perspective of stratosphere–troposphere exchange, *B. Am. Meteorol. Soc.*, 84, 1565–1573, doi:10.1175/BAMS-84-11-1565, 2003. 18163
- Stohl, A., Cooper, O. R., and James, P.: A Cautionary note on the use of meteorological analysis fields for quantifying atmospheric mixing, *J. Atmos. Sci.*, 61, 1446–1453, doi:10.1175/1520-0469(2004)061<1446:ACNOTU>2.0.CO;2, 2004. 18166
- 20 Stohl, A., Forster, C., Frank, A., Seibert, P., and Wotawa, G.: Technical note: The Lagrangian particle dispersion model FLEXPART version 6.2, *Atmos. Chem. Phys.*, 5, 2461–2474, doi:10.5194/acp-5-2461-2005, 2005. 18166
- Wang, P. H., Minnis, P., McCormick, M. P., Kent, G. S., and Skeens, K. M.: A 6-year climatology of cloud occurrence frequency from Stratospheric Aerosol and Gas Experiment II observations (1985–1990), *J. Geophys. Res.*, 101, 29407–29429, doi:10.1029/96JD02962, 1996. 18164
- 25 Winker, D. M. and Trepte, C. R.: Laminar cirrus observed near the tropical tropopause by LITE, *Geophys. Res. Lett.*, 25(17), 3351–3354, doi:10.1029/98GL01292, 1998. 18164
- WMO: Scientific Assessment of Ozone Depletion: 2006, Technical report no. 50, World Meteorological Organization, Geneva, 2007. 18163, 18166
- 30 Wohltmann, I. and Rex, M.: Improvement of vertical and residual velocities in pressure or hybrid sigma-pressure coordinates in analysis data in the stratosphere, *Atmos. Chem. Phys.*, 8, 265–272, doi:10.5194/acp-8-265-2008, 2008. 18166

A Lagrangian view of transport across the TTL

A. Tzella and B. Legras

[Title Page](#)[Abstract](#)[Introduction](#)[Conclusions](#)[References](#)[Tables](#)[Figures](#)[◀](#)[▶](#)[◀](#)[▶](#)[Back](#)[Close](#)[Full Screen / Esc](#)[Printer-friendly Version](#)[Interactive Discussion](#)

Wright, J. S., Fu, R., Fueglistaler, S., Liu, Y. S., and Zhang, Y.: The influence of summertime convection over South-East Asia on water vapor in the tropical stratosphere, *J. Geophys. Res.*, 116, D12302, doi:10.1029/2010JD015416, 2011. 18171, 18175

Discussion Paper | Discussion Paper | Discussion Paper | Discussion Paper | Discussion Paper

ACPD

11, 18161–18209, 2011

A Lagrangian view of transport across the TTL

A. Tzella and B. Legras

Title Page

Abstract

Introduction

Conclusions

References

Tables

Figures

⏪

⏩

◀

▶

Back

Close

Full Screen / Esc

Printer-friendly Version

Interactive Discussion



A Lagrangian view of transport across the TTL

A. Tzella and B. Legras

Table 1. Percentages of parcels that are “free” (i.e., have never encountered a convective source at the end of their 200-day back trajectory), “free” with initial locations in the extra-tropics (i.e., $|\phi| > 30^\circ$) and “free” with a range of values for the final potential temperatures, θ . Values correspond to the 100 hPa launch surface and those in parenthesis to the 70 hPa surface.

	ALLSKY- ΔT_0	ALLSKY- ΔT_5	ALLSKY- ΔT_{-5}	CLRSKY- ΔT_0
“free” parcels, %	17 (41)	18 (42)	15 (39)	23 (47)
“free” & $ \phi > 30^\circ$, %	15 (28)	15 (28)	14 (27)	17 (29)
“free” & $\theta > 400$ K, %	11 (30)	11 (31)	11 (30)	9 (25)
“free” & $380 < \theta < 400$ K, %	2 (3)	2 (4)	2 (4)	3 (5)
“free” & $\theta < 380$ K, %	3 (6)	4 (7)	2 (4)	11 (17)
“free” & $\theta < 360$ K, %	1 (2)	1.5 (2.7)	0.6 (1.3)	6 (8.5)

Title Page

Abstract

Introduction

Conclusions

References

Tables

Figures

⏪

⏩

◀

▶

Back

Close

Full Screen / Esc

Printer-friendly Version

Interactive Discussion



A Lagrangian view of transport across the TTL

A. Tzella and B. Legras

Table 2. Seasonal mean characteristics of convective sources and times for transport of air between detrainment and launch. Calculations made using the ALLSKY- $\Delta T0$ trajectory ensemble, launched at 100 hPa. The values for the median, $\mu_{1/2}$, and standard deviation, σ , are given in parenthesis.

	DJF	MAM	JJA	SON
CS-TTL parcels, %	27	27	22	23
Cloud temperature, K ($\mu_{1/2}$, σ)	205 (205, 9)	205 (205, 9)	205 (205, 9)	205 (205, 9)
Parcel potential temperature, K ($\mu_{1/2}$, σ)	354 (353, 3.72)	354 (353, 3.6)	357 (356, 6.2)	353 (352, 5.3)
Transit-time, days ($\mu_{1/2}$, σ)	59 (44, 47)	61 (46, 47)	62 (51, 43)	55 (42, 43)

Title Page

Abstract

Introduction

Conclusions

References

Tables

Figures

⏪

⏩

◀

▶

Back

Close

Full Screen / Esc

Printer-friendly Version

Interactive Discussion



A Lagrangian view of transport across the TTL

A. Tzella and B. Legras

Title Page

Abstract

Introduction

Conclusions

References

Tables

Figures

◀

▶

◀

▶

Back

Close

Full Screen / Esc

Printer-friendly Version

Interactive Discussion



Table 3. Same as Table 2 but this time the focus is on the regional mean characteristics of convective sources and transport times.

	Africa	N. Asian-Pacific	S. Asian-Pacific	C. America	S. America
CS-TTL parcels, %	10	22	50	6	5
Cloud temperature, K ($\mu_{1/2}$, σ)	201 (200, 8.6)	205 (205, 9.5)	206 (206, 8.7)	204 (204, 8.3)	203 (203, 7.4)
Parcel potential temperature, K ($\mu_{1/2}$, σ)	354 (354, 5.5)	357 (356, 5.5)	353 (352, 3.3)	353 (352, 5.4)	355 (353, 5.3)
Transit-time, days ($\mu_{1/2}$, σ)	61 (47, 46)	61 (50, 43)	58 (43, 46)	58 (45, 44)	61 (47, 46)

A Lagrangian view of transport across the TTL

A. Tzella and B. Legras

Title Page

Abstract

Introduction

Conclusions

References

Tables

Figures

◀

▶

◀

▶

Back

Close

Full Screen / Esc

Printer-friendly Version

Interactive Discussion



Table 5. Mean characteristics of the distributions of times for transport of cloud air out of the region below 360 K and into the 370 K and 380 K surface for the first time. Values obtained from the four CS-TTL trajectory ensembles, all launched at 100 hPa.

	ALLSKY- $\Delta T0$	ALLSKY- $\Delta T5$	ALLSKY- $\Delta T-5$	CLRSKY- $\Delta T0$
Exit-time from region below 360 K surface, days ($\mu_{1/2}$, σ)	15 (11, 16)	19 (13, 19)	12 (9, 13)	42 (32, 37)
First entry into 370 K surface, days ($\mu_{1/2}$, σ)	27 (23, 18)	31 (26, 20)	23 (20, 16)	54 (45, 37)
First entry into 380 K surface, days ($\mu_{1/2}$, σ)	39 (35, 22)	44 (39, 23)	33 (30, 20)	64 (56, 37)

A Lagrangian view of transport across the TTL

A. Tzella and B. Legras

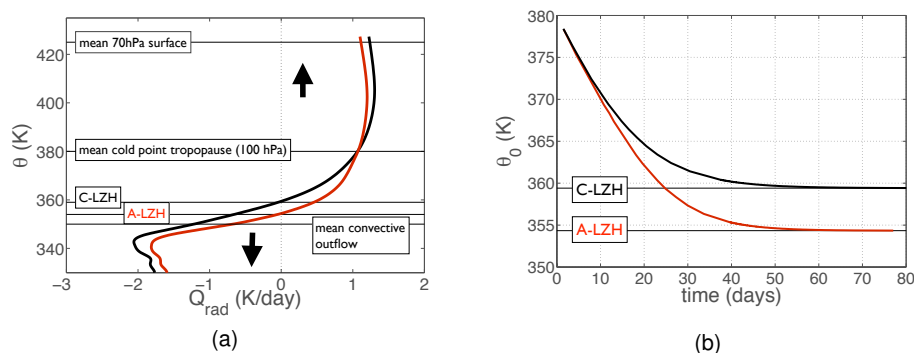


Fig. 1. (a) Annual mean tropical radiative heating rates (30° S, 30° N) calculated from all-sky (in red) and clear-sky (in black) radiative heating rates provided by the ERA-Interim dataset for 2005. (b) Transit-time from an initial level, θ_0 , to 380 K, calculated using the profiles shown in (a).

Title Page

Abstract

Introduction

Conclusions

References

Tables

Figures

◀

▶

◀

▶

Back

Close

Full Screen / Esc

Printer-friendly Version

Interactive Discussion



A Lagrangian view of transport across the TTL

A. Tzella and B. Legras

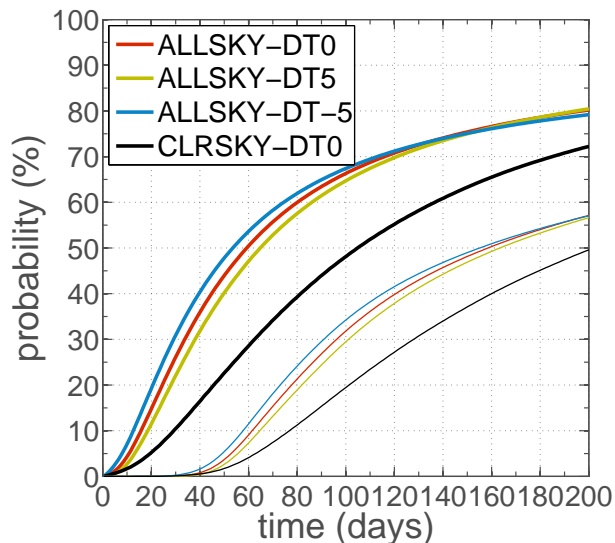


Fig. 2. Cumulative probability of time for transport of air between convective sources and the 100 hPa (thick lines) and 70 hPa (thin lines) surfaces. Results obtained from back trajectories, calculated in both clear-sky and all-sky conditions where different thermal biases were taken into account (see text for more details). The trajectories were launched between the beginning of 2005 and the middle of 2006.

Title Page

Abstract

Introduction

Conclusions

References

Tables

Figures

◀

▶

◀

▶

Back

Close

Full Screen / Esc

Printer-friendly Version

Interactive Discussion



A Lagrangian view of transport across the TTL

A. Tzella and B. Legras

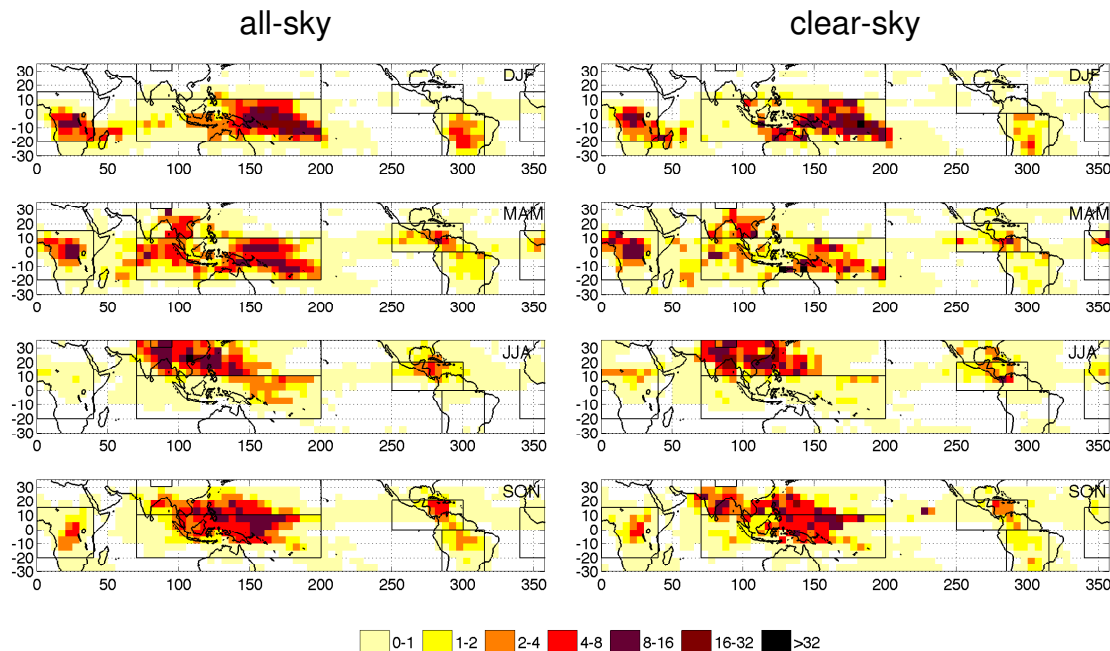


Fig. 3. Seasonal variations of the distribution, $\rho_{100 \text{ hPa}}$, of the horizontal locations where trajectories, initially launched at 100 hPa, have intersected clouds within the previous 200 days for the boreal winter (DJF), spring (MAM), summer (JJA), and fall (SON) seasons in 2005. The distributions on the left are calculated under all-sky conditions from the ALLSKY- ΔT_0 trajectory ensemble, while those on the right are calculated under clear-sky conditions, using the CLRSKY- ΔT_0 ensemble. The distributions are binned in a $5^\circ \times 5^\circ$ longitude/latitude grid. The solid boxes define a set of geographical regions. Africa: $(320^\circ, 20^\circ) \times (-15^\circ, 20^\circ)$; N. Asian-Pacific: $(70^\circ, 200^\circ) \times (10^\circ, 35^\circ)$; S. Asian-Pacific: $(70^\circ, 200^\circ) \times (-10^\circ, 10^\circ)$; C. America: $(250^\circ, 300^\circ) \times (0^\circ \text{ S}, 20^\circ)$; S. America: $(285^\circ, 315^\circ) \times (0^\circ, 35^\circ)$; Tibetan plateau: $(80^\circ, 95^\circ) \times (30^\circ, 35^\circ)$.

Title Page

Abstract Introduction

Conclusions References

Tables Figures

◀ ▶

◀ ▶

Back Close

Full Screen / Esc

Printer-friendly Version

Interactive Discussion



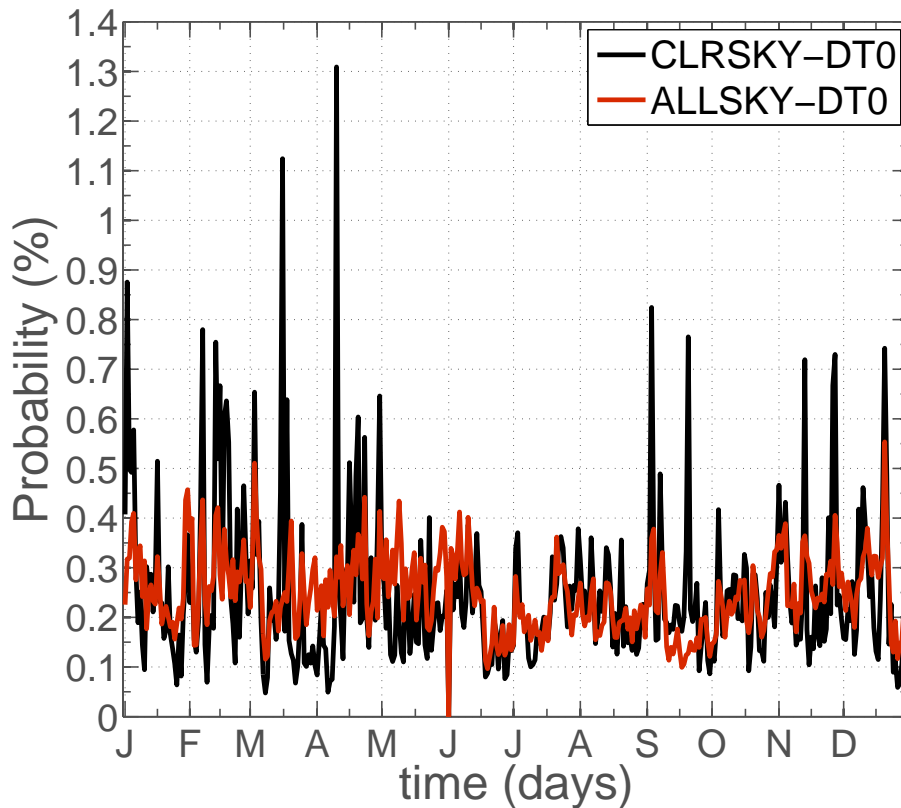


Fig. 4. Proportion of CS-TTL trajectories plotted as a function of their detrainment day. Proportion is calculated for transport in all-sky conditions from the ALLSKY- ΔT_0 ensemble (red) and for clear-sky conditions from the CLRSKY- ΔT_0 ensemble (black). Both ensembles are obtained from simulations launched at 100 hPa.

A Lagrangian view of transport across the TTL

A. Tzella and B. Legras

Title Page	
Abstract	Introduction
Conclusions	References
Tables	Figures
◀	▶
◀	▶
Back	Close
Full Screen / Esc	
Printer-friendly Version	
Interactive Discussion	



A Lagrangian view of transport across the TTL

A. Tzella and B. Legras

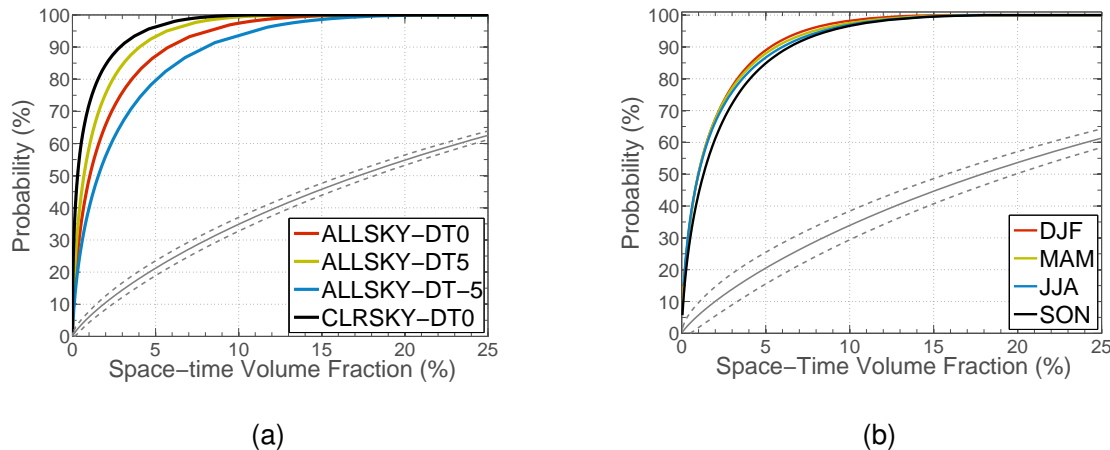


Fig. 5. (a) Ensemble and (b) seasonal differences between $\rho_{100 \text{ hPa}}$, measured by $P_{\rho}(\mathcal{A})$, defined in Eq. (2). The ensemble differences are calculated for all-sky and clear-sky conditions for trajectories launched at 100 hPa from the ALLSKY- $\Delta T0$, ALLSKY- $\Delta T5$, ALLSKY- $\Delta T-5$ and CLRSKY- $\Delta T0$, ensembles. ΔT denotes the different thermal biases for the brightness temperatures. Seasonal differences are calculated from the ALLSKY- $\Delta T0$ simulation by considering trajectories detrained during boreal winter (DJF), spring (MAM), summer (JJA) and fall (SON) seasons in 2005. For both (a) and (b) are plotted the average (solid grey) and mean \pm standard deviation (dotted grey) of $P_{\rho}(\mathcal{A})$. The latter is obtained from 1000 realisations of $\tilde{\rho}_{100 \text{ hPa}}$ trajectories are uniformly randomly distributed in both space and time. The same number of trajectories as ALLSKY- $\Delta T0$ are used in (a) and as many as those detrained during boreal winter are used in (b) – in practice this choice is not important as the ensemble and seasonal differences in the trajectory numbers are small.

A Lagrangian view of transport across the TTL

A. Tzella and B. Legras

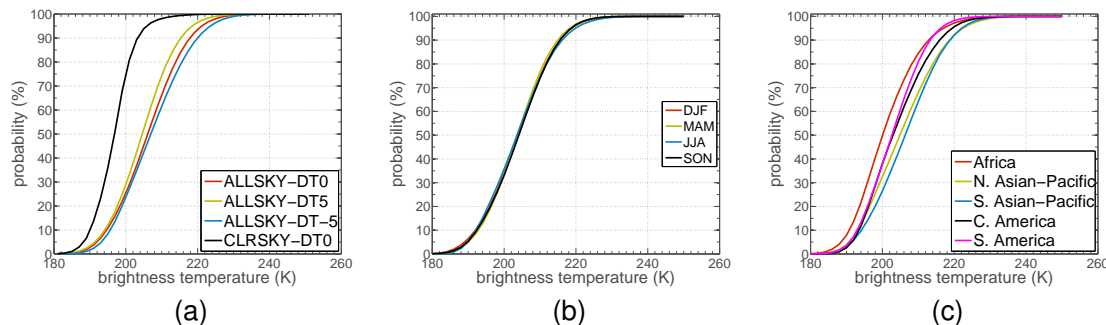


Fig. 6. Cumulative distributions of cloud top brightness temperatures for convective sources that transport air parcels to 100 hPa. Results obtained for **(a)** all-sky and clear-sky conditions, from trajectory ensembles ALLSKY- $\Delta T0$, ALLSKY- $\Delta T5$, ALLSKY- $\Delta T-5$ and CLRSKY- $\Delta T0$. Results obtained for all-sky conditions, from the ALLSKY- $\Delta T0$ ensemble, for trajectories detrained **(b)** during boreal winter (DJF), spring (MAM), summer (JJA) and fall (SON) seasons and **(c)** in the region of Africa, North Asian-Pacific, South Asian-Pacific, Central America and South America, designated in Fig. 3. All trajectories are launched at 100 hPa.

Title Page

Abstract

Introduction

Conclusions

References

Tables

Figures

◀

▶

◀

▶

Back

Close

Full Screen / Esc

Printer-friendly Version

Interactive Discussion



A Lagrangian view of transport across the TTL

A. Tzella and B. Legras

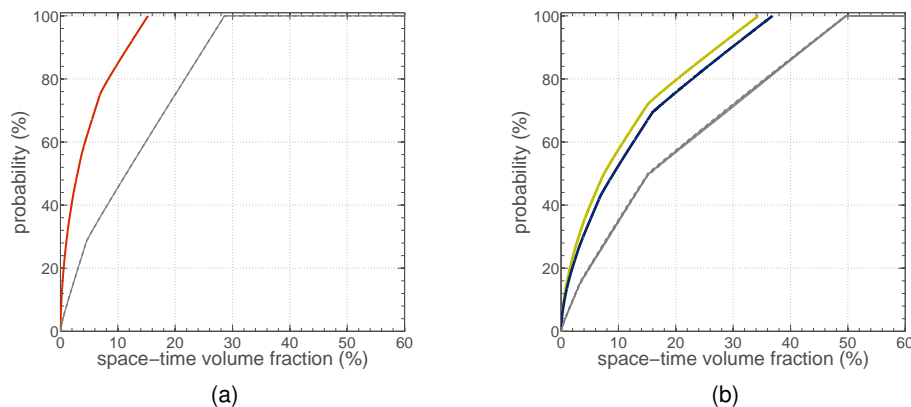


Fig. 7. Localization of horizontal distributions among sources of similar depth as measured by $P_{q|T^*}(\mathcal{A})$ obtained for **(a)** $T^* = 215$ K (red) and **(b)** 200 K (yellow) and 185 K (blue). The distributions are calculated for all-sky conditions, using the ALLSKY- $\Delta T0$ ensemble launched at 100 hPa. Also plotted the mean (solid grey) and mean \pm standard deviation (dashed grey) of $P_{q|T^*}(\mathcal{A})$ obtained from 1000 realisations of $\tilde{\rho}_{100 \text{ hPa}}$. The differences between the latter three curves is small for the range of values plotted here (see text for more details).

Title Page

Abstract

Introduction

Conclusions

References

Tables

Figures

◀

▶

◀

▶

Back

Close

Full Screen / Esc

Printer-friendly Version

Interactive Discussion



A Lagrangian view of transport across the TTL

A. Tzella and B. Legras

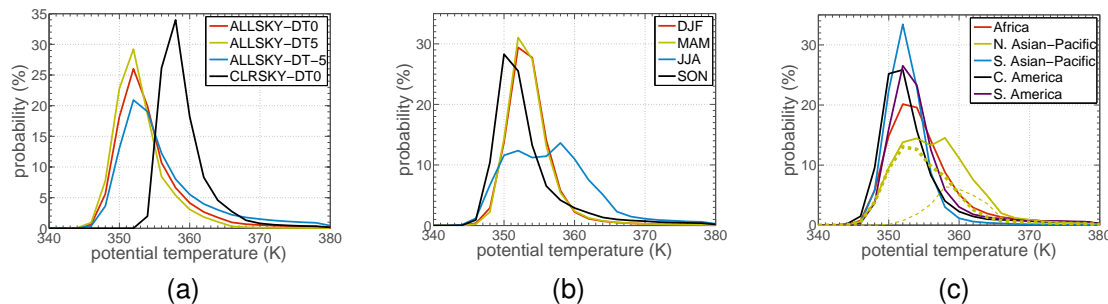


Fig. 8. Same as Fig. 6 but this time the focus is on the histograms of potential temperatures where air parcels have encountered a convective source.

Title Page

Abstract Introduction

Conclusions References

Tables Figures

◀ ▶

◀ ▶

Back Close

Full Screen / Esc

Printer-friendly Version

Interactive Discussion



A Lagrangian view of transport across the TTL

A. Tzella and B. Legras

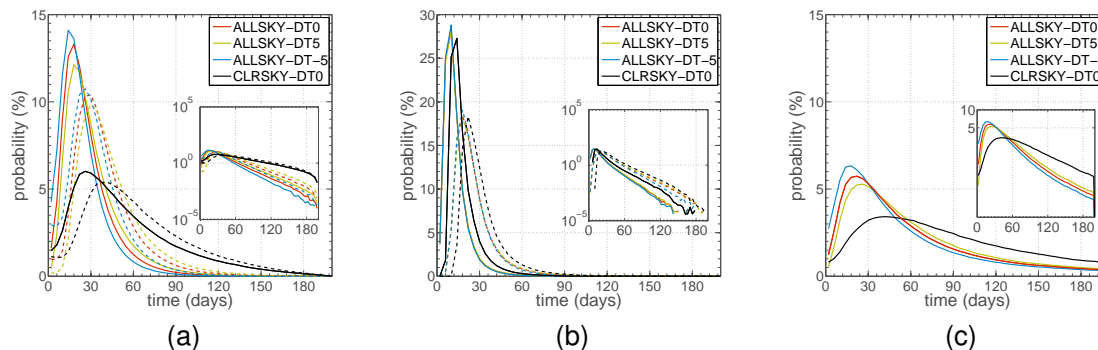


Fig. 9. Histograms showing **(a)** first-entry times of cloud air to the 370 K surface (solid) and 380 K surface (dotted) **(b)** times for cloud air to cross the 360–370 K layer (solid) and 360–380 K layer (dotted) and **(c)** transit-times between detrainment and launch. Results obtained for all-sky and clear-sky conditions from trajectory ensembles ALLSKY- $\Delta T0$, ALLSKY- $\Delta T5$, ALLSKY- $\Delta T-5$ and CLRSKY- $\Delta T0$, all launched at 100 hPa. The histograms are calculated using a bin size of 4 days.

[Title Page](#)
[Abstract](#)
[Introduction](#)
[Conclusions](#)
[References](#)
[Tables](#)
[Figures](#)
[◀](#)
[▶](#)
[◀](#)
[▶](#)
[Back](#)
[Close](#)
[Full Screen / Esc](#)
[Printer-friendly Version](#)
[Interactive Discussion](#)


A Lagrangian view of transport across the TTL

A. Tzella and B. Legras

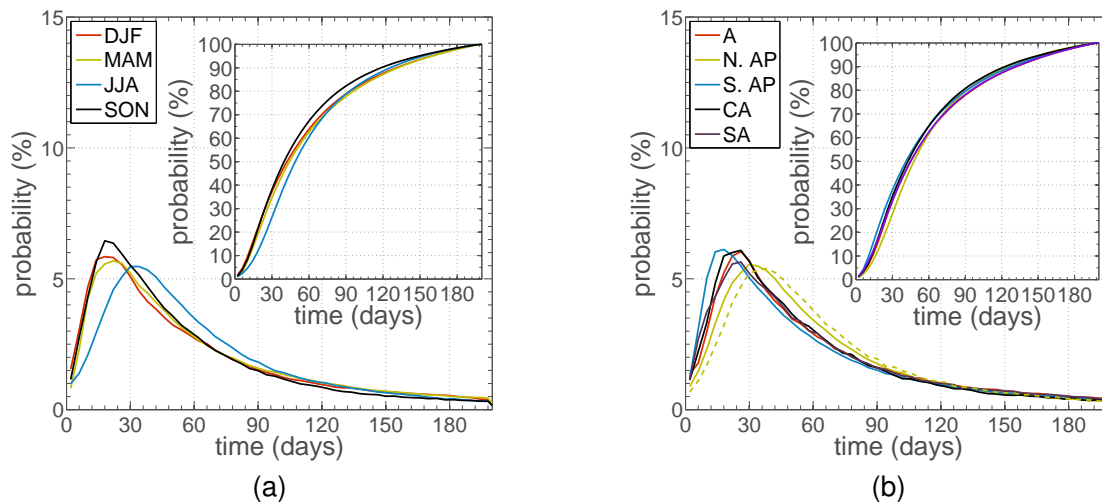


Fig. 10. (a) Seasonal and (b) regional variations of transit-times between detrainment and launch at the 100 hPa surface. Insets show the corresponding cumulative distributions. Also shown the corresponding histogram for those trajectories detrained over the land part of the North Asian-Pacific region (dashed). Results obtained from trajectory ensemble ALLSKY- $\Delta T0$. The histograms are calculated using a bin size of 4 days.

Title Page

Abstract

Introduction

Conclusions

References

Tables

Figures

◀

▶

◀

▶

Back

Close

Full Screen / Esc

Printer-friendly Version

Interactive Discussion



A Lagrangian view of transport across the TTL

A. Tzella and B. Legras

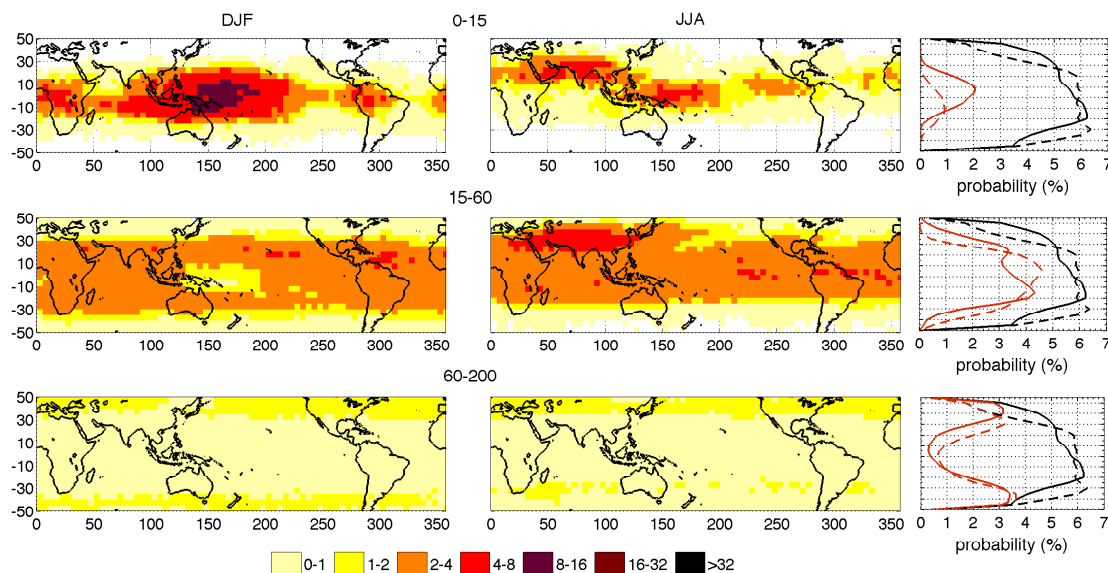


Fig. 11. Distribution, $\chi_{100 \text{ hPa}}$, of the horizontal locations of trajectories that have intersected clouds within the previous 15 days (top), between 15 and 60 days (middle) and between 60 and 200 days (bottom) on the 100 hPa launch surface. The distributions are calculated for trajectories detrained during the 2005 boreal winter (left) and boreal summer (middle) using the ALLSKY- ΔT_0 trajectory ensemble. The distributions are binned in a $5^\circ \times 5^\circ$ longitude/latitude grid and the histograms are calculated using a bin size of 5 degrees. The corresponding histograms showing the latitudinal position of CS-TTL trajectories detrained during boreal winter (solid) and summer (dotted) on the 100 hPa surface, both the total (in back) and as a function of different range of values for the transit-times, τ (in red).